A Demonstration of Artificial Dissipation Effects in Some Finite Volume Solution Methods for the Navier-Stokes Equation

by M.N. Macrossan and M.W. Hancock

Research Report No: 5/94

A DEMONSTRATION OF ARTIFICIAL DISSIPATION EFFECTS IN SOME FINITE VOLUME SOLUTION METHODS FOR THE NAVIER-STOKES EQUATIONS

M. N. Macrossan
M. W. Hancock

Department of Mechanical Engineering
University of Queensland
Australia 4072

Introduction

It is well known that numerical schemes for the solution of the governing equations of fluid mechanics can introduce errors which can be interpreted as arising from an artificial dissipation which is inherent in the solution method itself. Often the magnitude and nature of the inherent artificial dissipation cannot be quantified. It is the purpose of this work to present a method whereby the importance of the artificial dissipation can be readily estimated for a particular flow situation.

The method is to simulate a viscous heat conducting flow where the dissipative properties of the simulated fluid *arise entirely from the numerical method* itself. This is done by applying a standard Navier-Stokes computational method to a particular problem, but specifying that the viscosity and thermal conductivity of the fluid are zero everywhere throughout the flow *except at solid wall boundaries.* At solid wall boundaries the usual no-slip and thermally conducting surface condition is applied with the assumption that the fluid just at the surface has the viscosity and thermal conductivity which is correct for the problem under consideration.

With the fluid viscosity and thermal conductivity set to zero the numerical method should produce a solution of the Euler equations for an ideal fluid but with the boundary conditions appropriate to a dissipative fluid, if such a thing is possible. It would appear that a singularity should develop near the surface; that is, vorticity and energy would be injected into the flow by the wall boundary condition and, since there should be no way for these quantities to dissipate away from the wall in an ideal fluid, vorticity and energy should accumulate to infinite or

non-physical values.

However, in practice, no such singularity appears and the results for the flow of this entirely artificial fluid can look convincing if the solution method itself is highly dissipative. It is a wise precaution to inspect the predicted flow of the artificially dissipative fluid and compare it with the flow predicted by the computational method working in its normal mode. For example, if the thickness of boundary layer developed in the artificial fluid is large compared to the boundary layer thickness predicted by the computational method in its normal mode it is clear that the artificial dissipation is not negligible and the method is not reliable for this particular problem.

The Navier-Stokes equations in Finite Volume Form

Consider a space (x,y,z) divided into N contiguous elements of volume V_j for $j = 1,N$. Let S be the surface of V_j and $\hat{\mathbf{n}}$ the outward normal and let the unit vectors $\hat{\mathbf{p}}$ and $\hat{\mathbf{q}}$ form, with $\hat{\mathbf{n}}$, an orthogonal set of local axes at the surface S. Denote the components of the local fluid velocity $\mathbf{v}$ relative to these axes as (v_n, v_p, v_q). The Navier-Stokes equations for the conservation of mass, momentum and energy in integral or control volume form can be written for each volume V_j as

$$\frac{\partial}{\partial t}\int_{V_j} \mathbf{U}\, dV + \int_S (\mathbf{F}_E + \mathbf{F}_D)\, dS = 0 \qquad (1)$$

where the conserved quantities (/unit volume) are

$$\mathbf{U} = \begin{pmatrix} \rho \\ \rho v_n \\ \rho v_p \\ \rho v_q \\ \rho(\frac{1}{2} \mathbf{v}^2 + e_{int}) \end{pmatrix} \qquad (2)$$

For brevity in (2) we have not written the necessary transformation of momentum from a varying set of axes (n-p-q) attached to a surface element of the control volume to a global fixed set of axes.

The fluxes across S are written in two parts; the *Euler* fluxes

$$\mathbf{F}_E = \begin{pmatrix} \rho v_n \\ \rho v_n v_n + \rho RT \\ \rho v_n v_p \\ \rho v_n v_q \\ \rho v_n\{1/2\mathbf{v}.\mathbf{v} + \gamma RT/(\gamma-1)\} \end{pmatrix}, \tag{3}$$

and the *dissipative* fluxes

$$\mathbf{F}_D = \begin{pmatrix} 0 \\ -\tau_{nn} \\ -\tau_{np} \\ -\tau_{nq} \\ -(v_n\tau_{nn} + v_p\tau_{np} + v_q\tau_{nq}) + \phi_n \end{pmatrix}. \tag{4}$$

In (2) e_{int} is the specific internal energy and a perfect gas equation of state, $p = \rho RT = \rho(\gamma - 1)e_{int}$ where R is the ordinary gas constant, has been assumed.

The τ_{nj} in (4) are the stresses (excluding the thermodynamic pressure) acting on the surface S and ϕ_n is the component of the heat flux vector normal to S. These are related to the strains in the fluid by the constitutive relations

$$\tau_{nn} = (4\mu/3 + \mu_B)\partial v_n/\partial x_n + (\mu_B - 2\mu/3)(\partial v_p/\partial x_p + \partial v_q/\partial x_q) \tag{5}$$

$$\tau_{np} = \mu(\partial v_n/\partial x_p + \partial v_p/\partial x_n) \tag{6}$$

$$\tau_{nq} = \mu(\partial v_n/\partial x_q + \partial v_q/\partial x_n) \tag{7}$$

$$\phi_n = -\kappa\, \partial T/\partial x_n, \tag{8}$$

where μ is the coefficient of dynamic viscosity, μ_B is the co-efficient of bulk viscosity, κ is the thermal conductivity and (x_n, x_p, x_q) are position coordinates measured in the directions of the unit vectors $\hat{\mathbf{n}}$, $\hat{\mathbf{p}}$ and $\hat{\mathbf{q}}$ attached to the surface S.

The Euler equations can be obtained from (1) by putting $\mathbf{F}_D = 0$, that is, the Euler equations described the flow of an ideal fluid which has zero viscosity and thermal conductivity.

Construction of a Navier-Stokes Solver

It is common to construct a Navier-Stokes solver by taking an Euler solver and adding in the appropriate Navier-Stokes dissipative fluxes. A finite volume shock capturing method for the Euler equations will make some estimate of the Euler fluxes which could be written as $\mathbf{F}_E + \mathbf{F}_A$ to show that this estimate will contain some errors which are in effect artificial dissipative terms $\mathbf{F}_A$ added to the correct Euler fluxes $\mathbf{F}_E$. When the Navier-Stokes dissipative terms are added the final flux terms become $\mathbf{F}_E + \mathbf{F}_A + \mathbf{F}_D$ (where we have ignored any error in the estimation of $\mathbf{F}_D$). Clearly, for the Navier-Stokes solver to be accurate we require that $|\mathbf{F}_A| << |\mathbf{F}_D|$.

We next demonstrate, for a test flow, the effect of the artificial dissipation inherent in three different finite volume Navier-Stokes solvers, each based on a different method of estimating the Euler fluxes.

Test Case: Compressible Flow over a Flat plate.

The test case is that used by Jacobs (1991), Mallett (1993) and Macrossan and Oliver (1993) to test some finite volume Navier-Stokes codes. The body is a flat plate aligned parallel to the freestream velocity. The freestream Mach number and temperature are $M_1 = 2$ and $T_1 = 222$ K and the wall temperature is fixed at $T_w = T_1$. A perfect gas with a ratio of specific heats of $\gamma = 1.4$ is assumed and the viscosity of the gas is given by a Sutherland viscosity law

$$\mu = \mu_0 \ (T/T_0) \quad (T_0 + S_v)/(T + S_v) \tag{9}$$

where μ_o and T_0 are references quantities and $S_v = 110.4$ K is a constant. The thermal conductivity is given by

$$k = C_p \ \mu/Pr \tag{10}$$

where C_p is the specific heat at constant pressure and $Pr = 0.72$ is the constant Prandtl number. The freestream Reynolds number based on the plate length L was $Re_L = 1.65 \times 10^5$.

A spectral boundary layer solution, which was obtained by Jacobs using

the method of Pruett and Street (1991), is available for this case. The temperature profile across the boundary layer at the station x/L = 0.916 is shown in figure 1. We take a measure of the boundary layer thickness to be $\Delta = 3y_T$, where y_T gives the location of the peak temperature in the boundary layer. For the spectral solution the boundary layer thickness is $\Delta/x = 13.3 \times 10^{-3}$.

It was shown in earlier work (Macrossan & Oliver 1993), and it will become apparent here, that it is reasonable to take this spectral solution as being close to the exact solution, except for a slight error in the boundary condition at the edge of the boundary layer; the spectral solution has boundary conditions imposed at the edge of the boundary layer which are equal to the freestream conditions. In contrast, the finite volume solutions capture the weak oblique leading edge interaction shock (which is generated by the displacement effect of the boundary layer). Hence the conditions at the edge of the boundary layer are slightly different from the freestream conditions.

Comparison of three finite volume methods

The three methods for calculating the Euler fluxes which are considered here are: (1) the Equilibrium Flux Method (Pullin 1980); (2) a Godunov scheme using an approximate Riemann solver (Jacobs 1991); and the Equilibrium Interface Method (Macrossan & Oliver 1993). A single code was used which had available the options of using any of these three methods to calculate the Euler fluxes and also the option of invoking first or second order spatial accuracy when estimating the Euler fluxes. Second order accurate estimates of the gradients of flow properties necessary to determine the Navier-Stokes dissipative fluxes were calculated as described by Macrossan and Oliver (1993). A simple rectangular grid was used, as in Macrossan and Oliver (1993), and the cells sizes varied in the positive x and y directions in an arithmetic progression . The ratio of the smallest to largest cell size in both directions was 10 in all cases.

The methods have different degrees of accuracy as can be seen in Fig. 2 which shows the temperature variation through the boundary layer as calculated by using the different methods. These results were obtained using the spatially *first order* method. The grid is the same in each case;

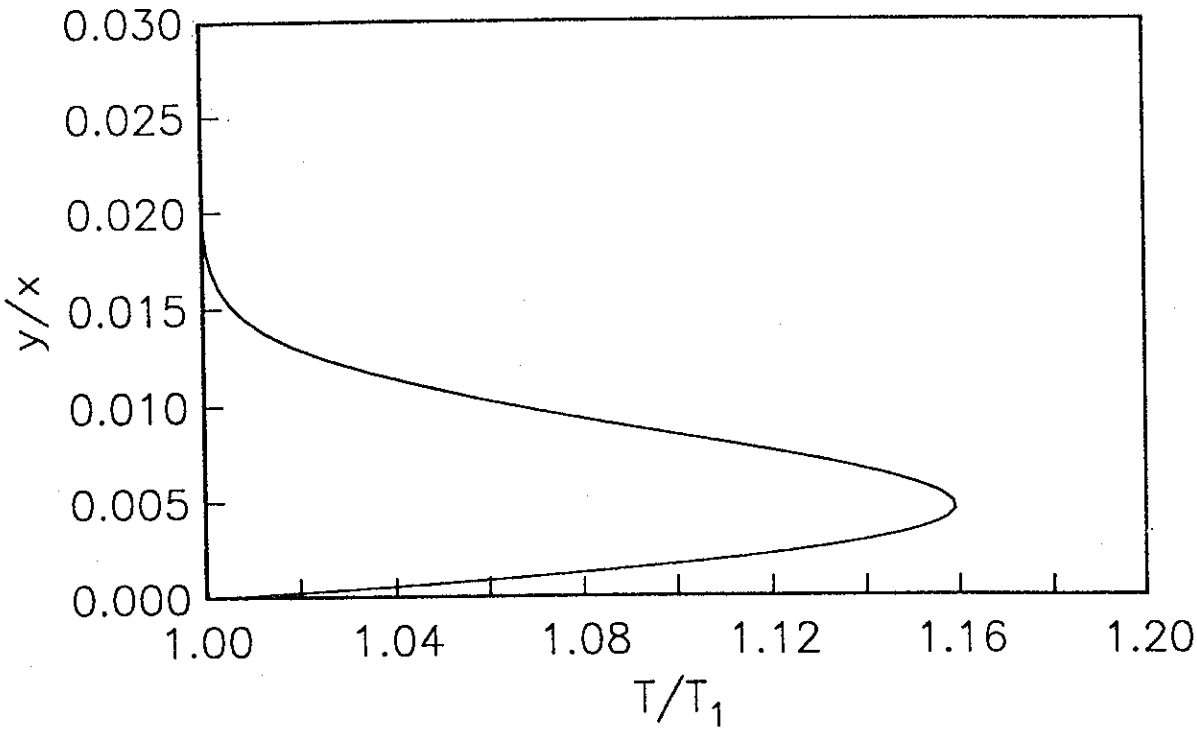

Fig. 1. Spectral solution for temperature in the boundary layer at x/L = 0.916. M_1 = 2.0. Re_L = 1.65x10^5. T_1 = T_w = 222 K.

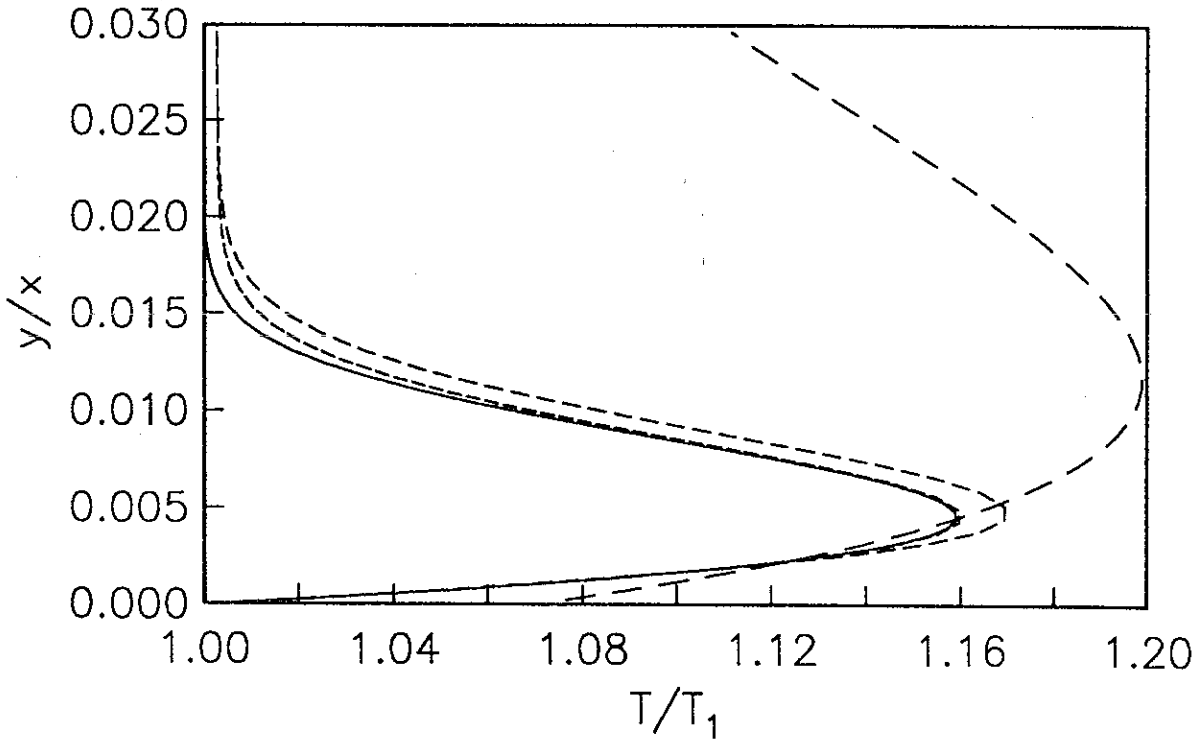

Fig. 2. First order finite volume methods compared with spectral solution of fig. 1. - - -, EIM; — — —, Riemann solver; —— —— ——, EFM. (52x252).

the smallest cell size in the y direction was $\Delta y \cong 5 \times 10^{-4}$ L and there were approximately 25 cells across the boundary layer thickness. It can be seen that EIM and the Riemann solver give much better agreement with the spectral solution than does EFM. The boundary layer thickness in each case was: EIM $\Delta/x = 13.0 \times 10^{-3}$; Riemann $\Delta/x = 15.5 \times 10^{-3}$; EFM $\Delta/x = 33.9 \times 10^{-3}$. The results for the second order versions of all these methods are shown in fig. 3. The boundary layer thickness in each case is: EIM $\Delta/x = 11.9 \times 10^{-3}$; Riemann $\Delta/x = 12.3 \times 10^{-3}$; EFM $\Delta/x = 20.6 \times 10^{-3}$.

Artificially Dissipative Flows

To demonstrate the inherent artificial dissipation directly we can show how a boundary layer develops when the no-slip, heat conducting boundary condition is applied at the plate surface and when the fluxes terms everywhere else consist only of the approximation to the Euler fluxes. The results for the second order EFM method are shown in fig. 4. The inherent dissipation induces a boundary layer of thickness $\Delta/x = 13 \times 10^{-3}$, which is comparable to boundary layer thickness predicted by the spectral method (although the shape of the profile is different) which is some 75% of the boundary layer thickness developed predicted by the solver in its normal mode. It is clear that the inherent dissipation in EFM is of a magnitude comparable to the Navier-Stokes dissipation which we are attempting to model.

In contrast to EFM the other two methods have a relatively small inherent artificial dissipation. Figure 5 shows the boundary layer developed from the inherent dissipation in the first and second version of the Riemann solver method. This boundary layer for the artificial fluid is much thinner than that shown in the spectral solution. The temperature has fallen to below $1.01T_w$ within 7 cells from the surface for the first order calculation and within 5 cells for the second order calculation.

Figure 6 shows the boundary layer developed from the inherent dissipation in both first and second EIM, on a coarser grid than was used for the Riemann solver method and EFM (the cell size was doubled in each direction). The temperature has fallen to below $1.01T_w$ within 5 cells from the surface for the first order calculation and within 4 cells for the second order calculation.

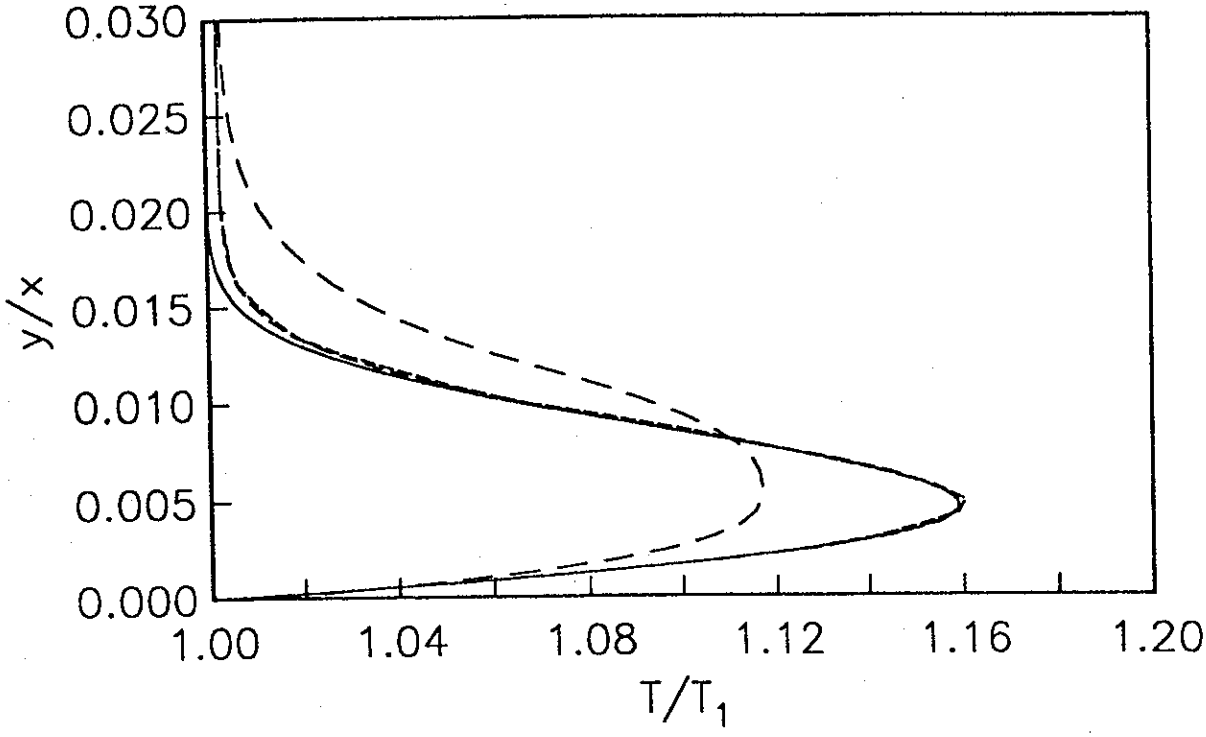

Fig. 3. Second order finite volume methods compared with spectral solution of fig. 1. - - -, EIM; — — —, Riemann solver; —— —— ——, EFM. (52x252)

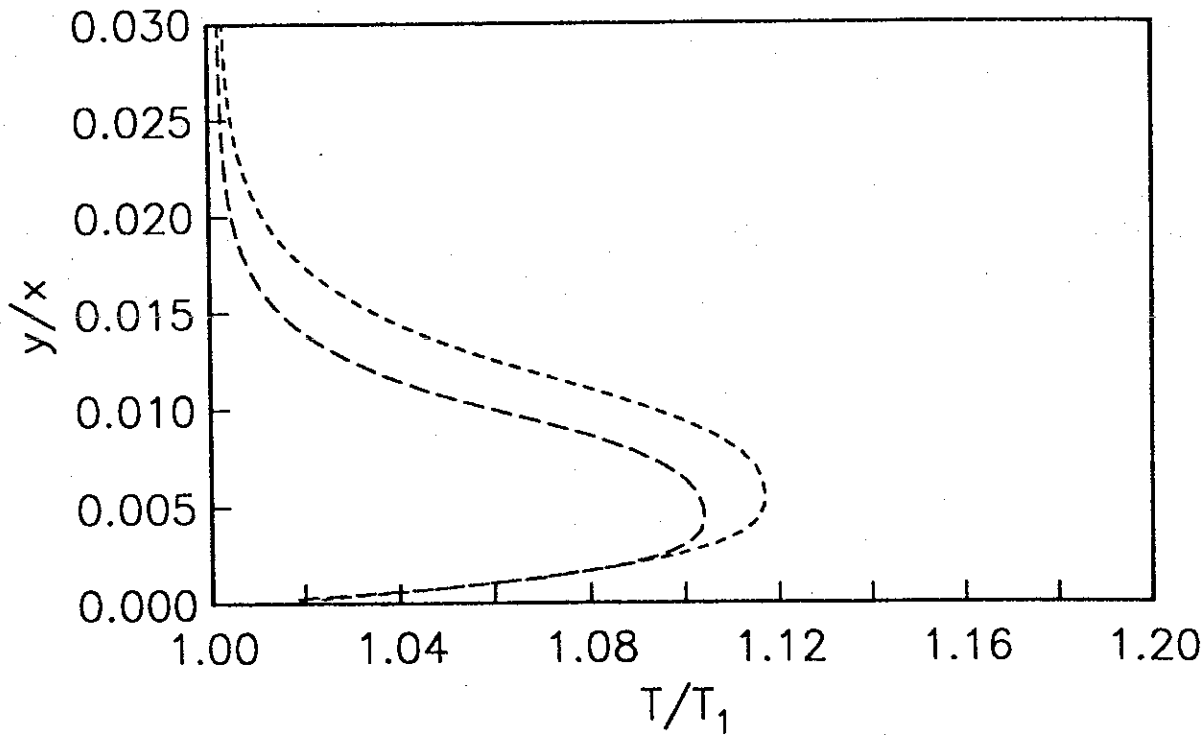

Fig. 4. EFM second order calculations for no slip and heat conducting wall boundary condition, with (- - -) and without (— — —) Navier-Stokes dissipative fluxes. (52x252).

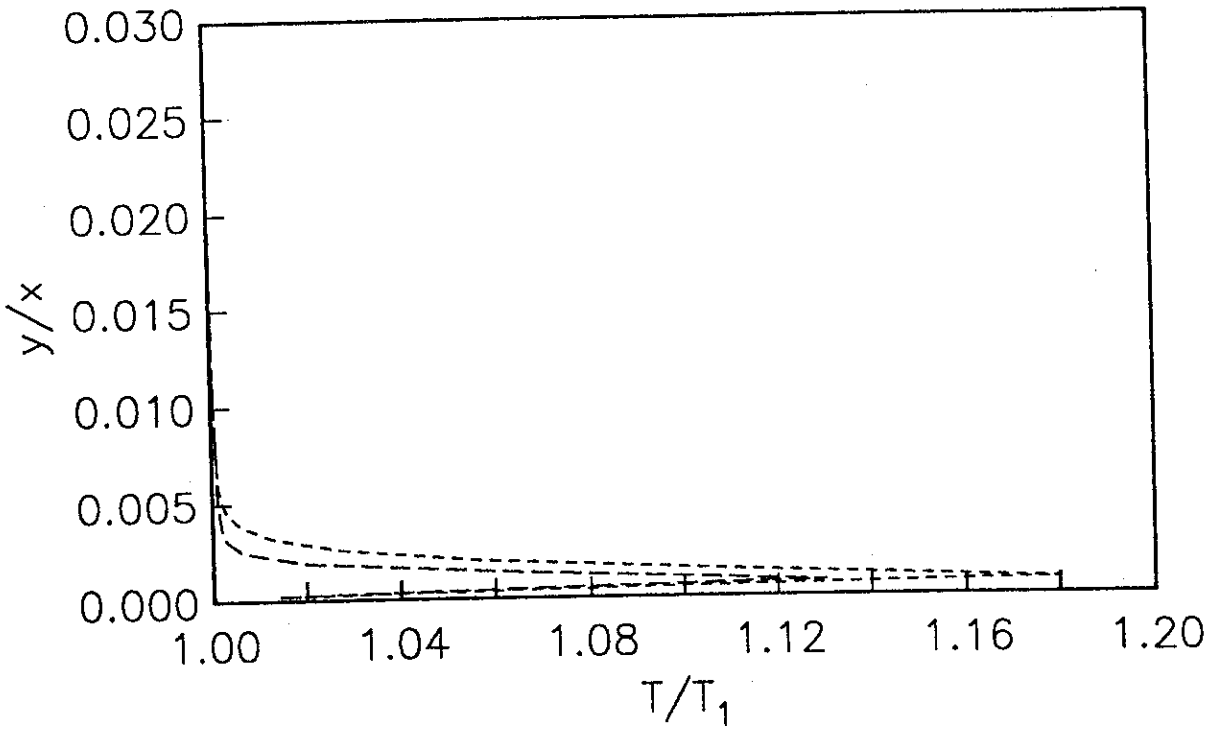

Fig. 5. Inherent dissipation flows for first and second order Riemann solver method. (52x252).

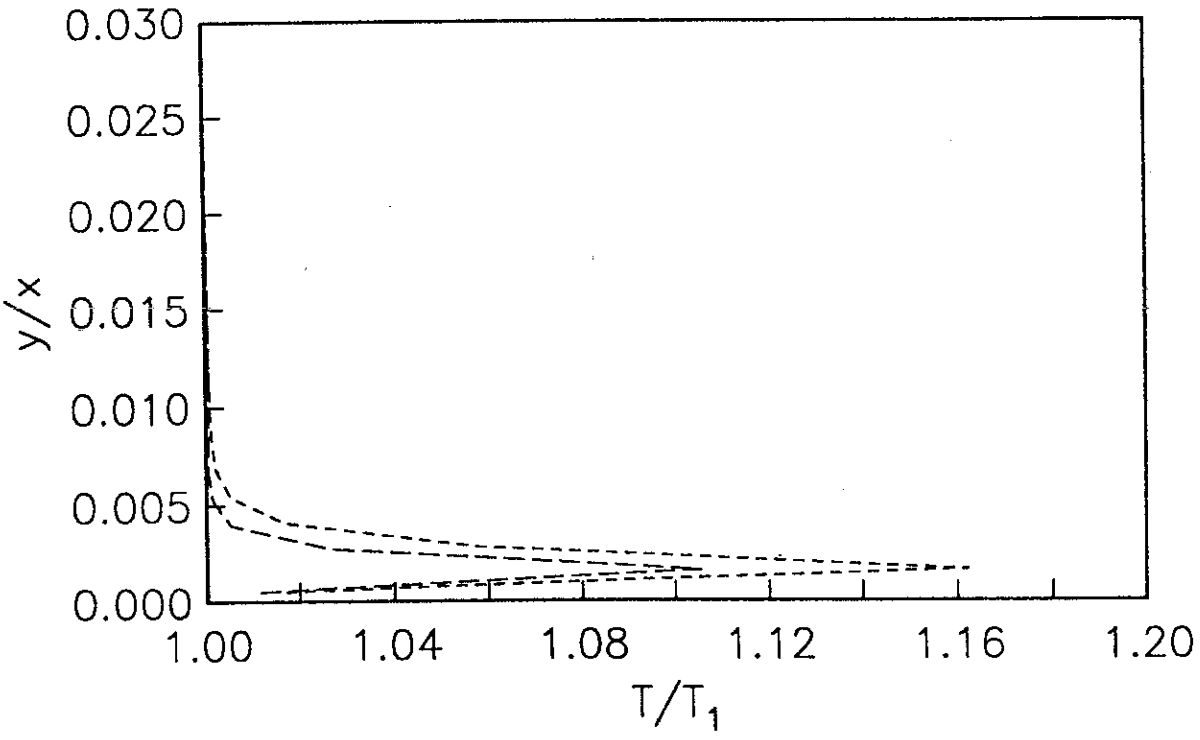

Fig. 6. Inherent dissipation flows for first and second order EIM. (26x126).

Limiting Solutions

We can attempt to show the artificial dissipation effects in EFM by the conventional method of obtaining a solution on successively more refined grids in the expectation that the artificial dissipation will decrease with the square of the characteristic cell size (for second order EFM). The solution should approach the correct limiting solution as the cell size approaches zero. A series of runs was performed on different grids (some grids were constructed by sub-division of the coarser grids in the y direction only and others by sub-division in both the x and y directions). Figure 7 shows that the EFM results are approaching the spectral solution but the best EFM results are still some way from the spectral solution.

The results for two grids (52x400 and 52x800) can be used to estimate the limiting solution using what is known as Richardson extrapolation. This is based on the idea that a second order accurate solution method will produce and estimate S_e of the solution which is related to the exact or limiting solution S_{lim} by

$$S_e(\delta x) \cong S_{lim} + A\ \delta x^2 + \textit{higher order terms} \qquad (11)$$

where δx is a characteristic size of the computational cells and A is a constant which depends on the problem being solved and the solution method itself.

If we consider two grids which have characteristic cell sizes of δx and $2\delta x$, eq. (11) can be written for both cases and solved for $A\ \delta x^2$ to get

$$A\ \delta x^2 \cong 1/3\ [S_e(2\delta x) - S_e(\delta x)] + \textit{higher order terms} \qquad (12)$$

It follows that if the solutions on the two grids are known an estimate of the limiting solution can be obtained as

$$S_{lim} \cong 4/3\ S_e(\delta x) - 1/3\ S_e(2\delta x). \qquad (13)$$

Because of the neglected higher order terms in (12) the estimated solutions $S_e(\delta x)$ and $S_e(2\delta x)$ need to be reasonable close to the limiting solution for eq. (13) to give a good estimate of the limiting solution (Ferziger 1989).

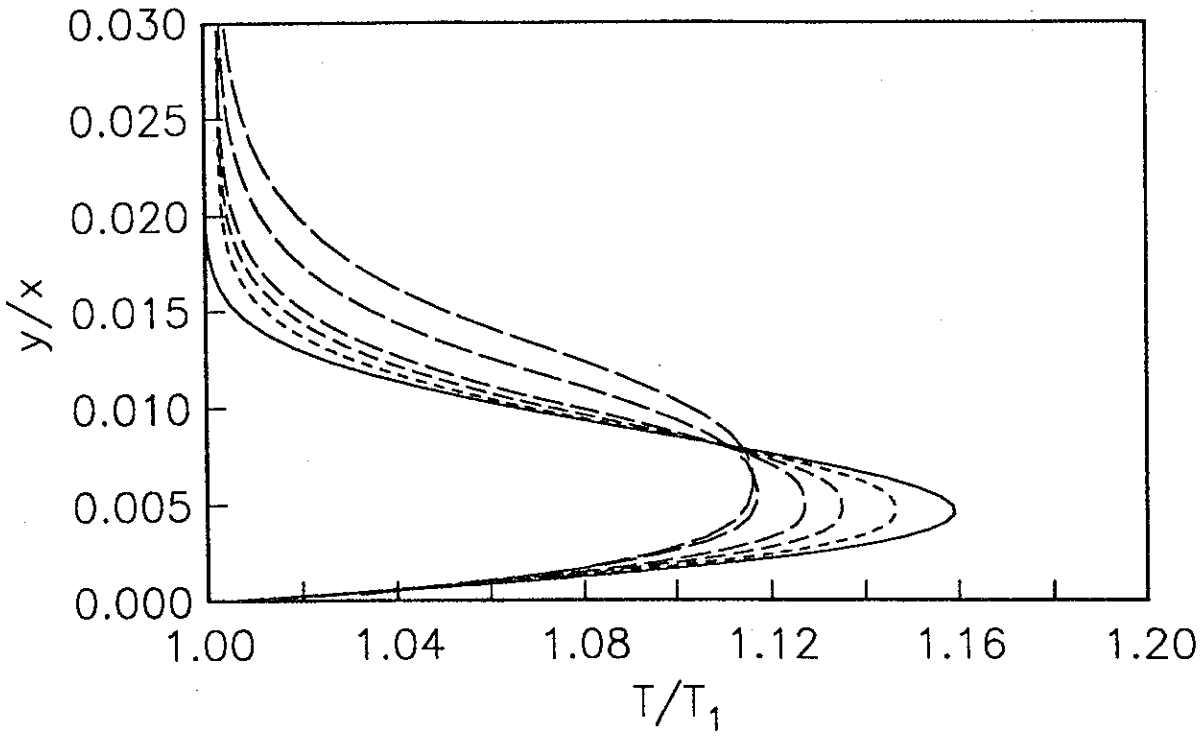

Fig. 7. Solutions for second order EFM on different grids compared with the spectral solution: ——— ———, 52x200; ——— ———, 52x252; — —, 52x400; — —, 104x504; - - -, 52x800; ———, spectral solution.

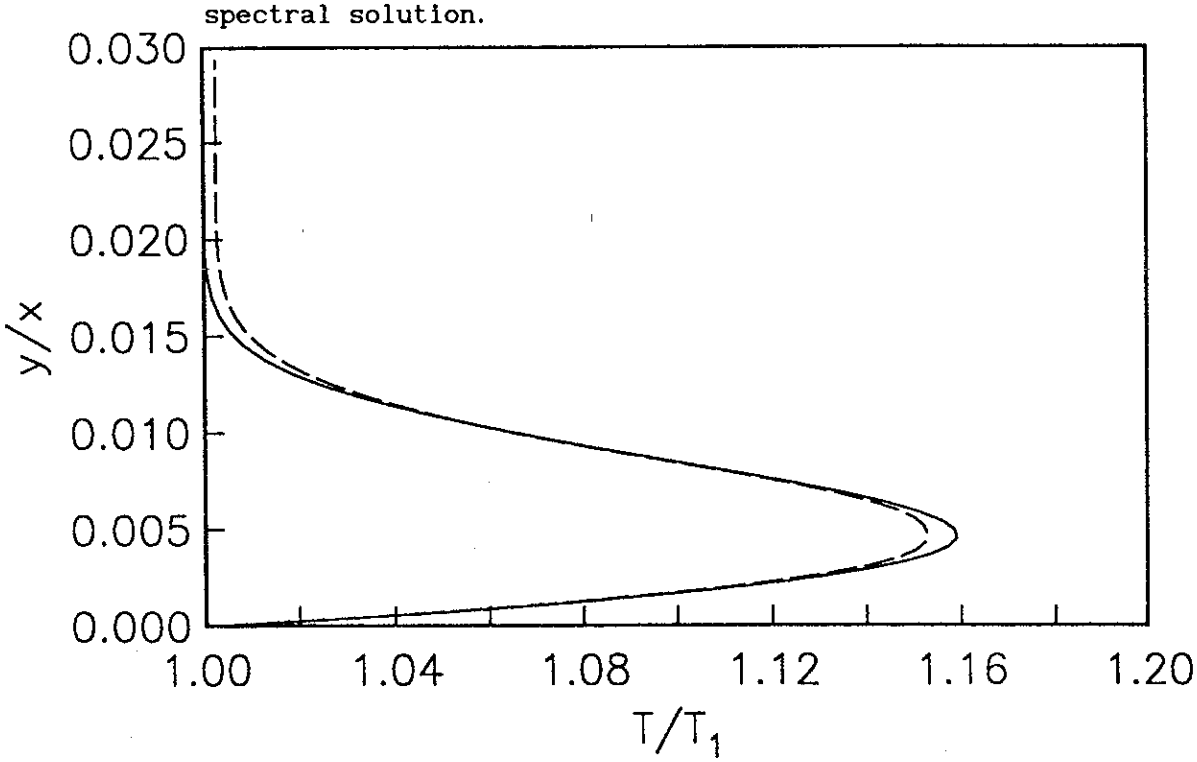

Fig. 8. Richardson extrapolated limit for second order EFM compared with the spectral solution.

Figure 8 shows the Richardson extrapolated limit for EFM derived from two of the curves in figure 7 and this extrapolated limit is indeed reasonably close to the spectral solution. For comparison some limiting curves obtained by Richardson extrapolation from the Riemann solver method and EIM are shown in figure 9.

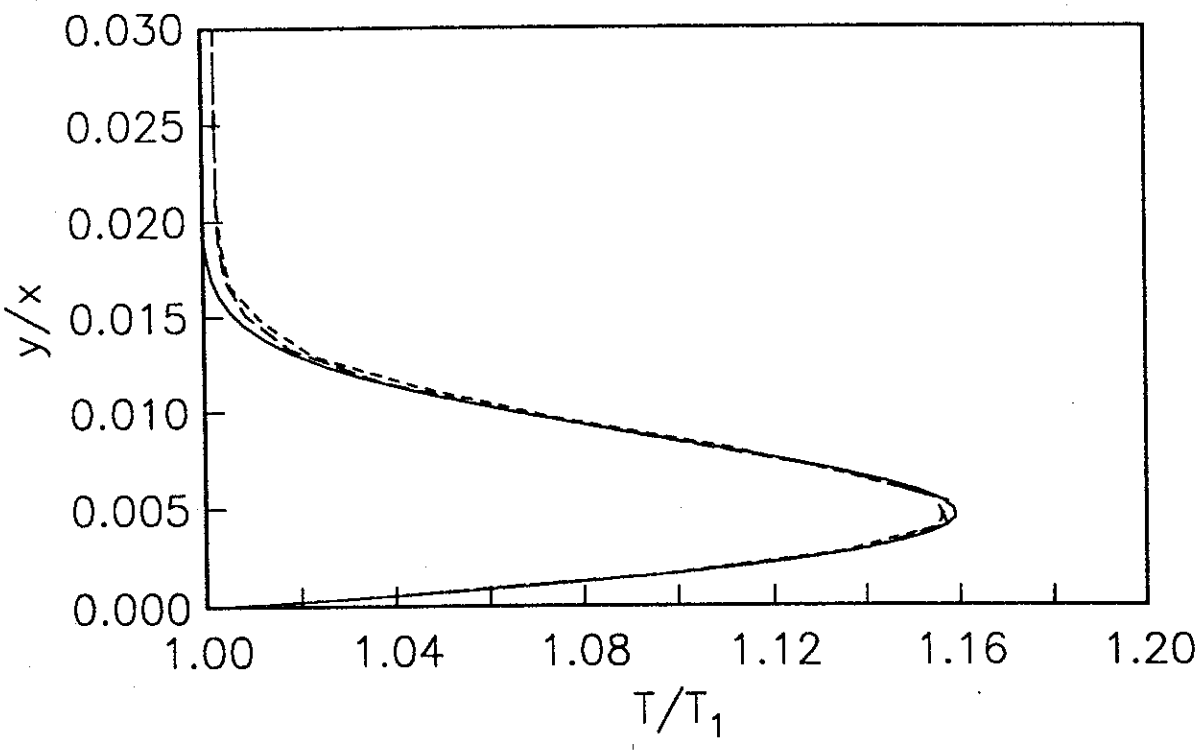

Fig. 9. Richardson extrapolated limits (26x126 & 52x252) for second order Riemann solver method and EIM compared with the spectral solution: — —, Riemann solver; - - -, EIM; ———, spectral solution.

Conclusion

A method of illustrating the effects of artificial dissipation in a solution method for the Navier-Stokes equations has been proposed. In this method a flow solution is developed in which the dissipation is that inherent in the method itself, except at the surface, where the transfer of momentum and heat across the wall is determined from the true viscosity and heat conductivity of the fluid being simulated. A boundary layer develops, and the thickness of this boundary layer compared to the thickness of

boundary layer predicted by the method working in its normal mode gives a graphic illustration of how much the artificial dissipation itself can be affecting the solution.

The results here indicate that second order EFM is much more dissipative than other methods. These other methods are known to be somewhat less stable than EFM (Hancock 1994) and EFM may continue to be used in some situations. Before using any method to solve the Navier-Stokes equations in any new application it would be wise to find the artificially viscous solution and compare this to the estimated Navier-Stokes solution.

References

Ferziger, J. H. 1989, *Forum on Methods of Estimating Uncertainty Limits in Flow Computations,* ASME Winter Annual Meeting, San Francisco, Dec 1989.

Hancock, M. W. 1994, *M. Eng. Sci. Thesis*, Department of Mechanical Engineering, University of Queensland.

Jacobs, P. A. 1991, *NASA CR-187613, ICASE Interim Report 18*, July 1991.

Macrossan, M. N. and Oliver, R. I. 1993, *Int J Numer Meth Fluid.* **17**, 177.

Mallett, E. R. 1993, *Ph. D. Thesis*, Department of Mechanical Engineering, University of Queensland.

Pullin, D. I. 1980, *J. Comput. Phys.* **34**, 231.

Pruett, C. D. and Street, C. L. *Int J Numer Meth Fluid.* **13**, 713.

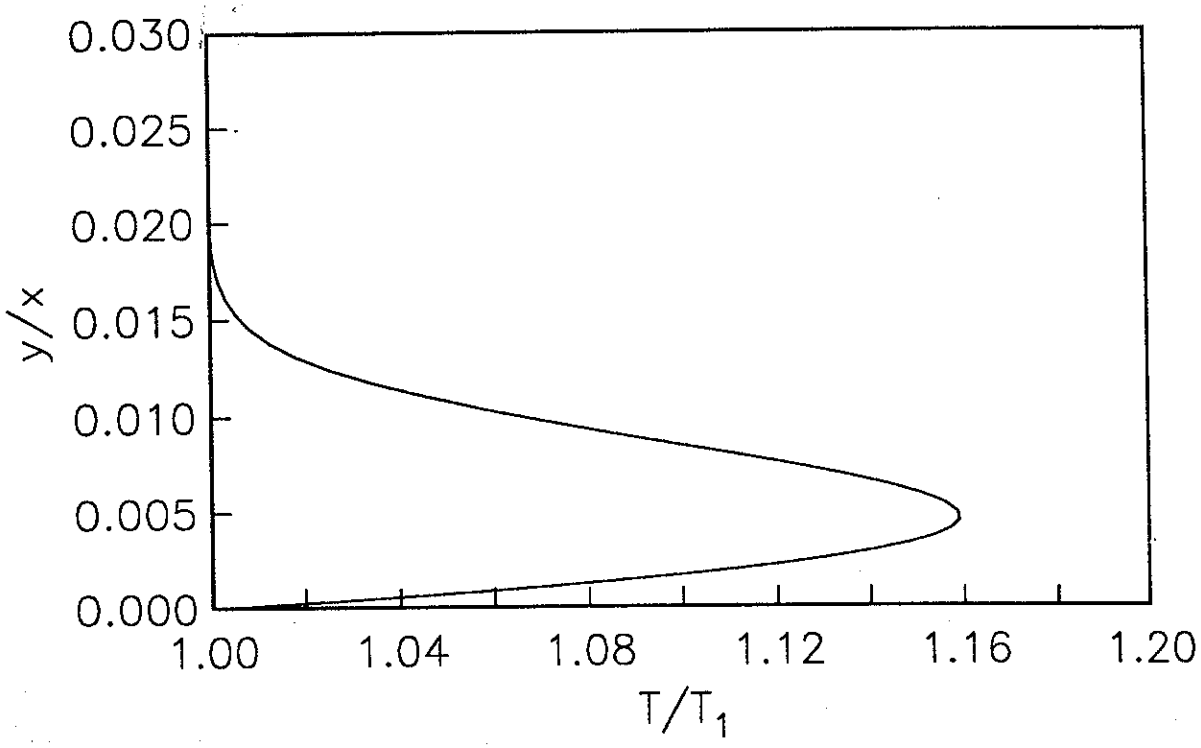

Fig. 1. Spectral solution for temperature in the boundary layer at x/L = 0.916. M_1 = 2.0. $Re_L = 1.65 \times 10^5$. $T_1 = T_w$ = 222 K.

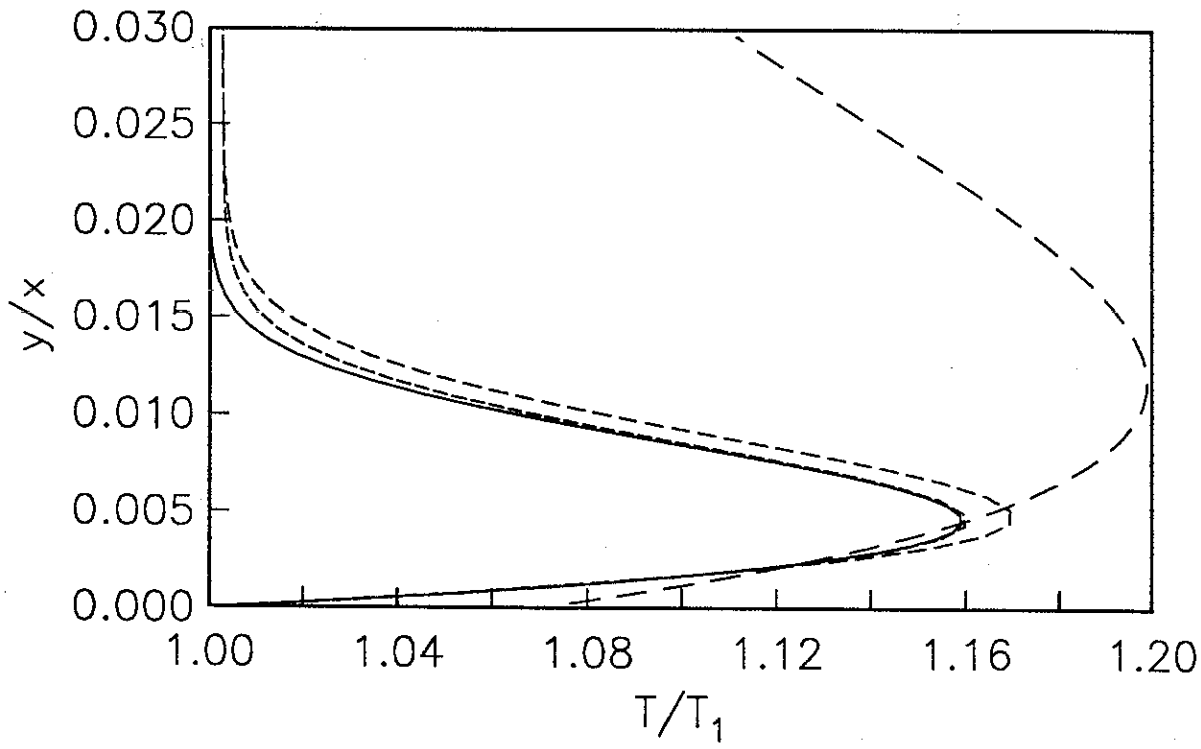

Fig. 2. First order finite volume methods compared with spectral solution of fig. 1. - - -, EIM; — — —, Riemann solver; ——— ——— ———, EFM. (52x252).

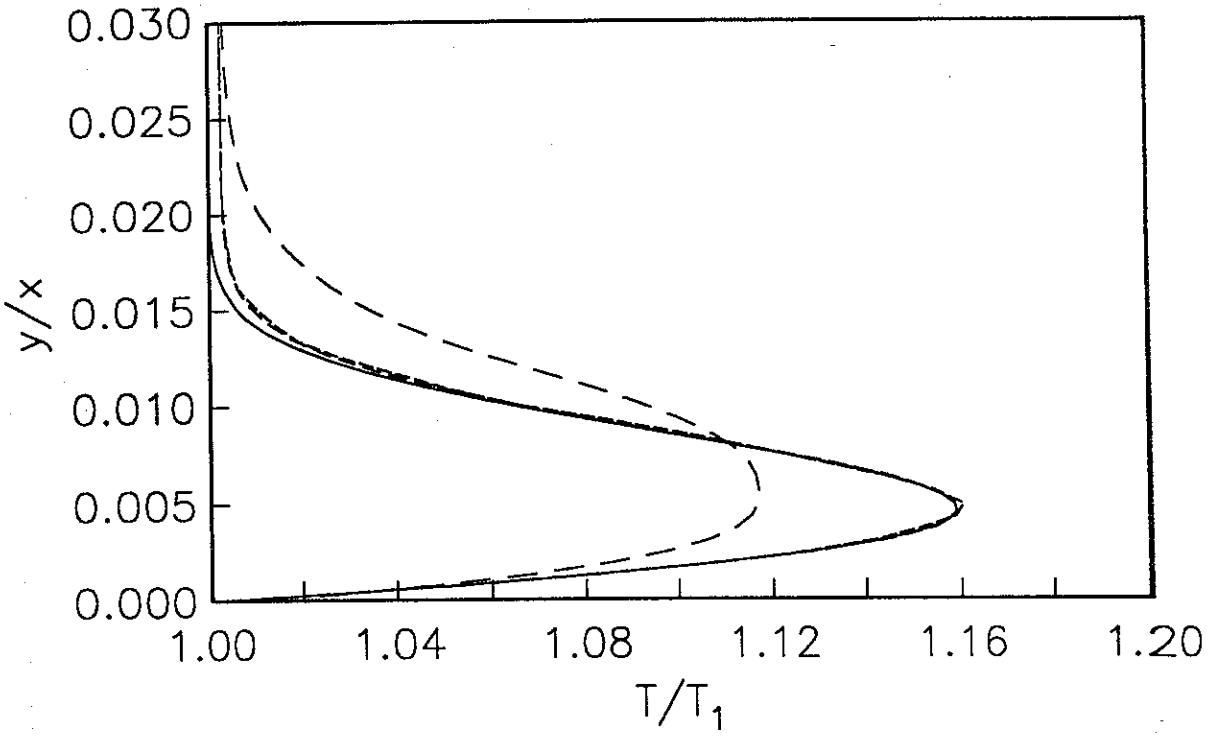

Fig. 3. Second order finite volume methods compared with spectral solution of fig. 1. - - -, EIM; — — —, Riemann solver; —— —— ——, EFM. (52x252)

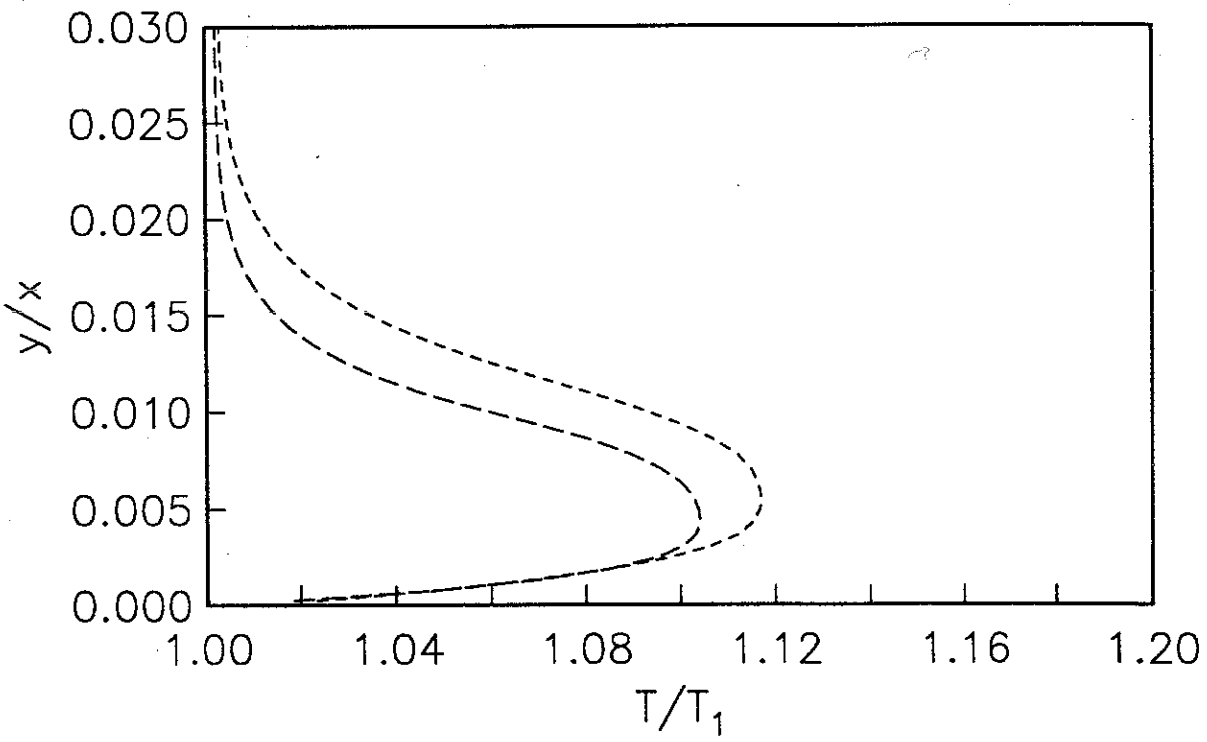

Fig. 4. EFM second order calculations for no slip and heat conducting wall boundary condition, with (- - -) and without (— — —) Navier-Stokes dissipative fluxes. (52x252).

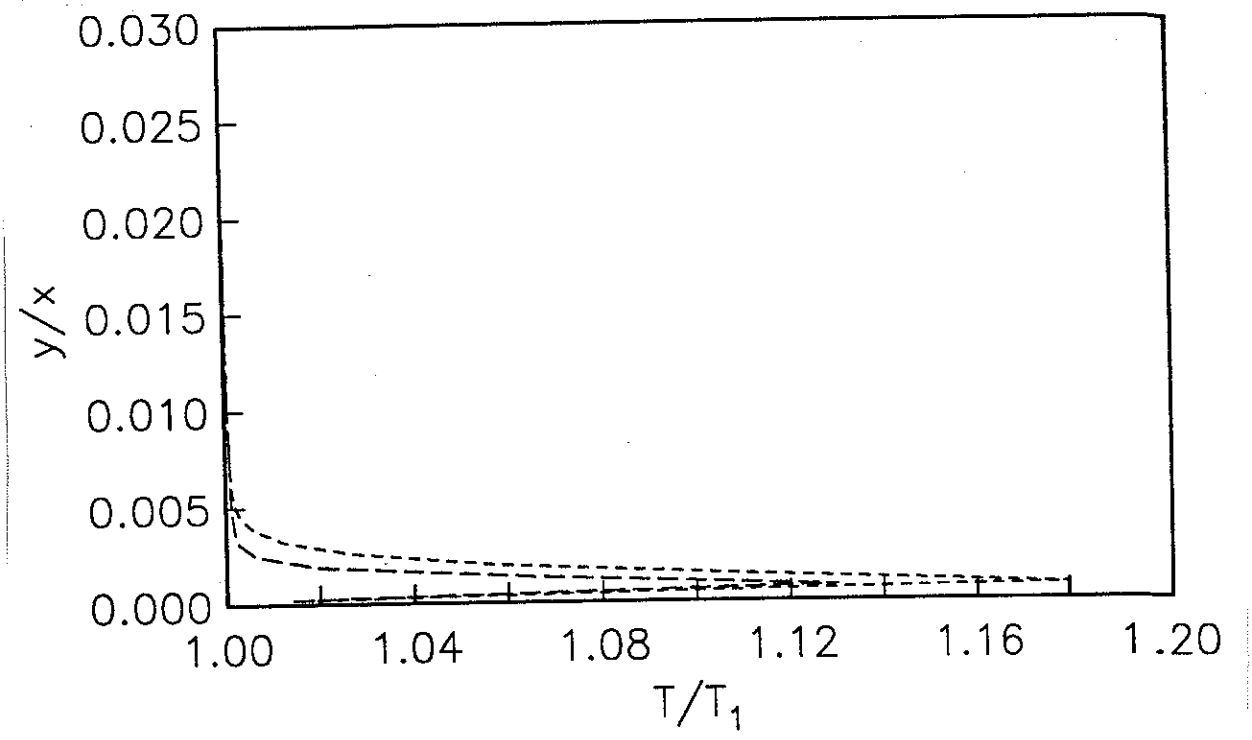

Fig. 5. Inherent dissipation flows for first and second order Riemann solver method. (52x252).

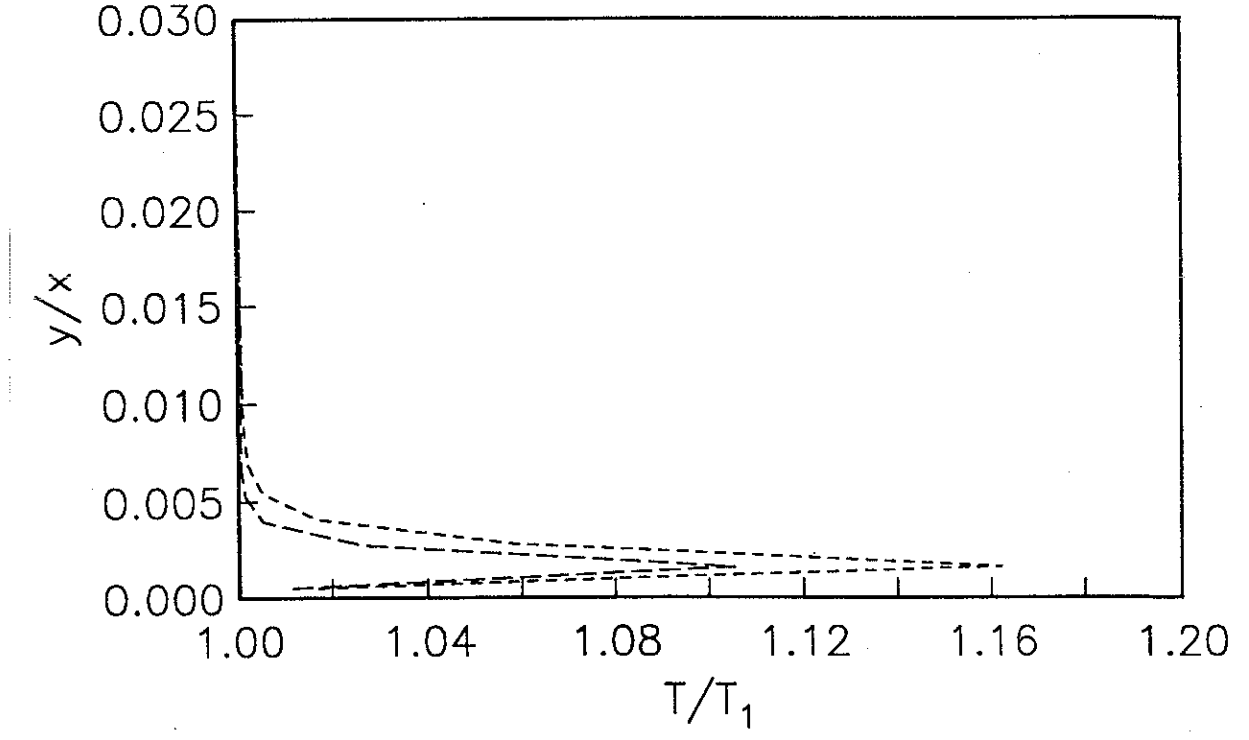

Fig. 6. Inherent dissipation flows for first and second order EIM. (26x126).

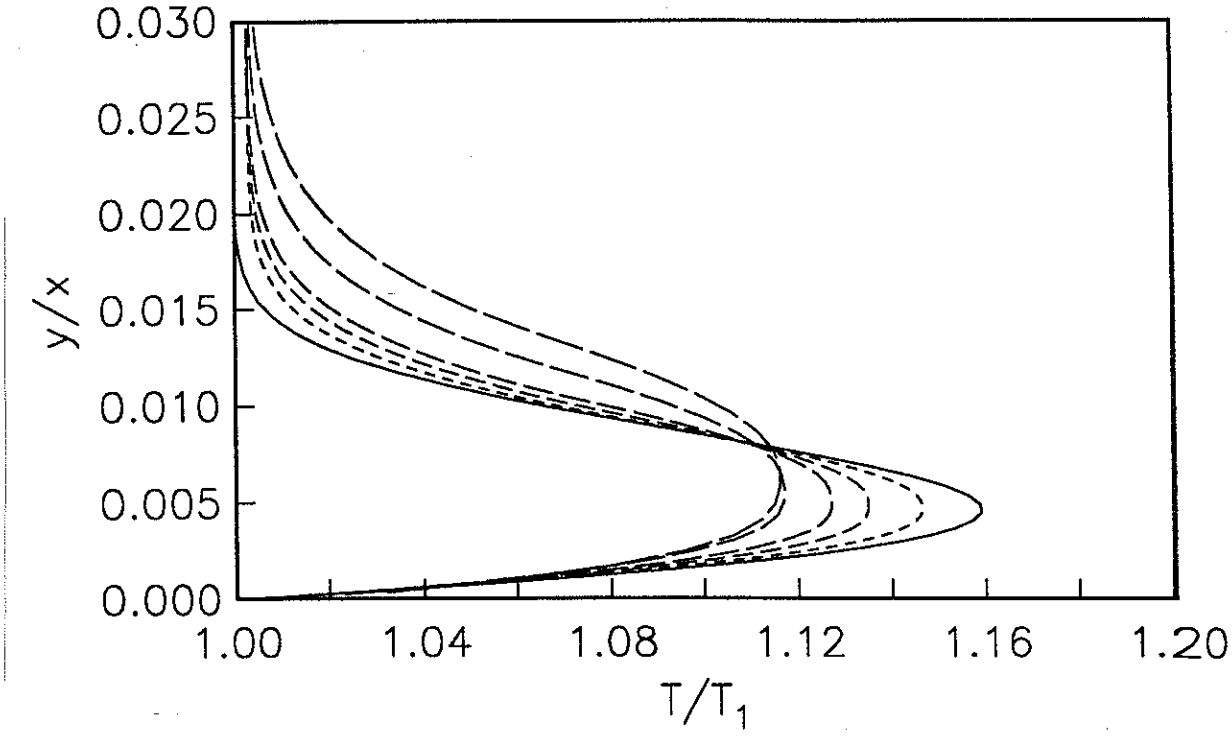

Fig. 7. Solutions for second order EFM on different grids compared with the spectral solution: ——— ———, 52x200; ——— ———, 52x252; — —, 52x400; — —, 104x504; - - -, 52x800; ———, spectral solution.

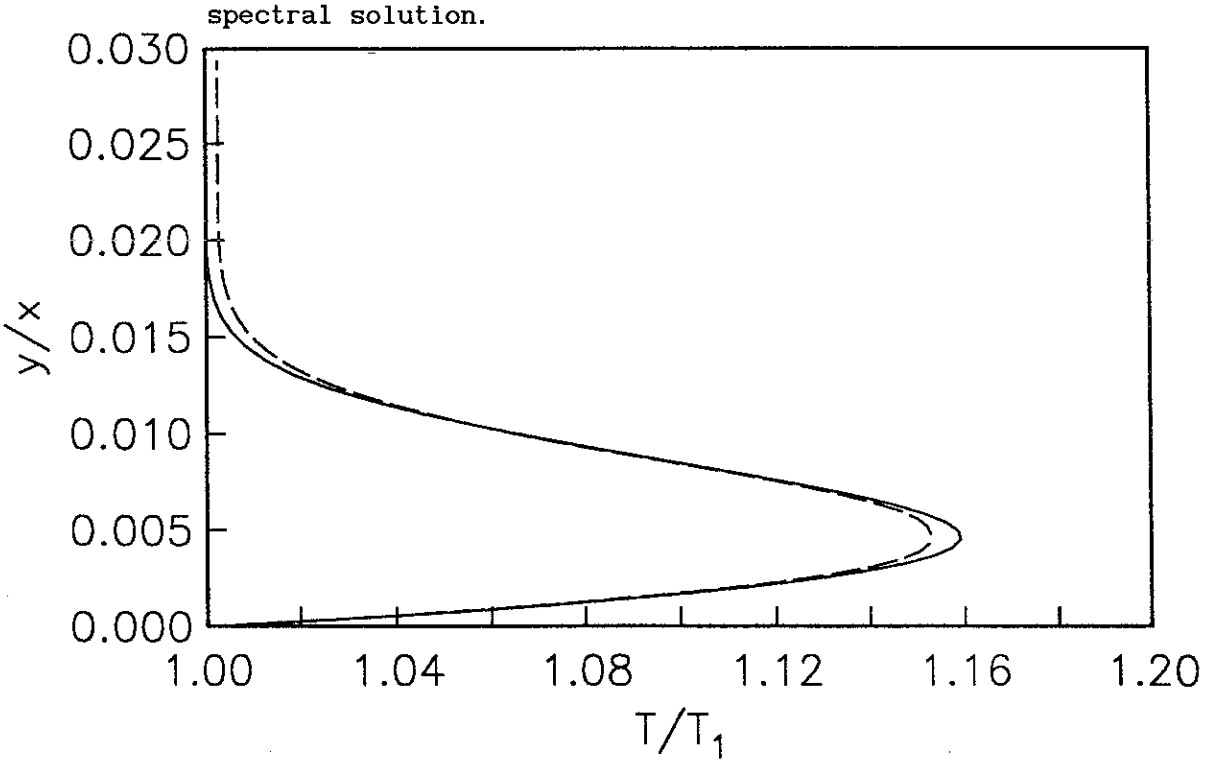

Fig. 8. Richardson extrapolated limit for second order EFM compared with the spectral solution.

Figure 8 shows the Richardson extrapolated limit for EFM derived from two of the curves in figure 7 and this extrapolated limit is indeed reasonably close to the spectral solution. For comparison some limiting curves obtained by Richardson extrapolation from the Riemann solver method and EIM are shown in figure 9.

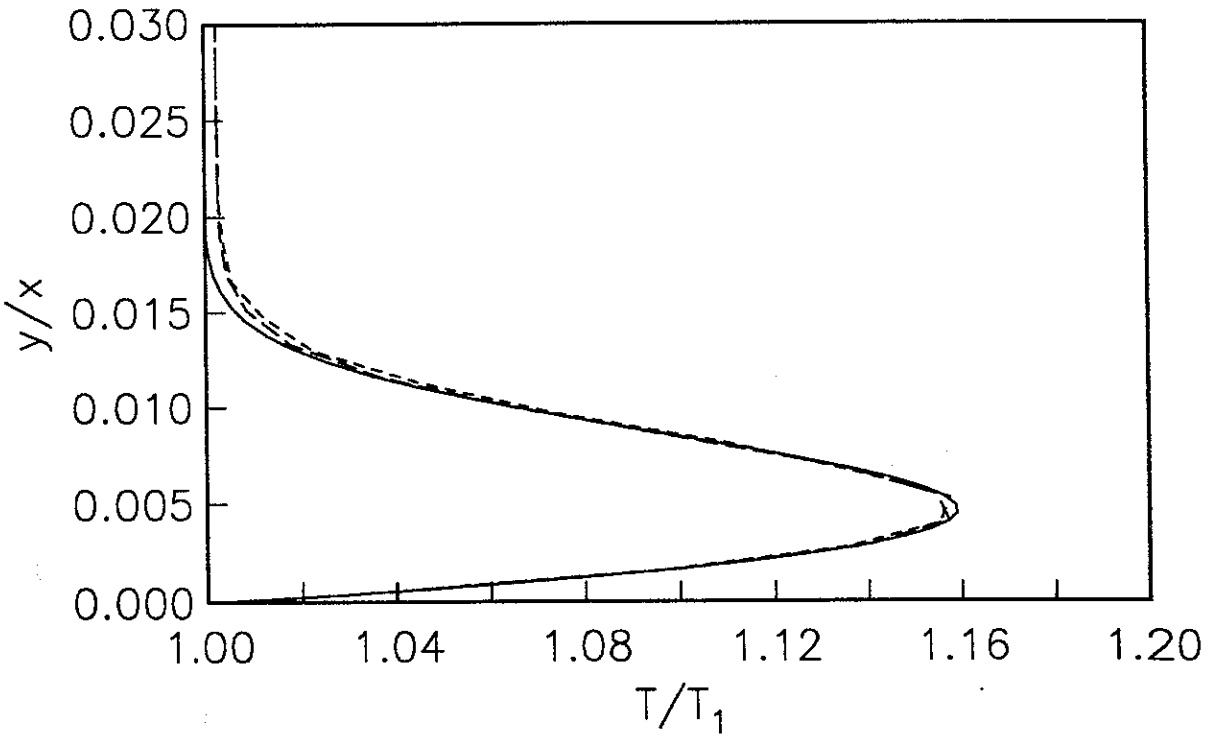

Fig. 9. Richardson extrapolated limits (26x126 & 52x252) for second order Riemann solver method and EIM compared with the spectral solution: — —, Riemann solver; - - -, EIM; ———, spectral solution.

Conclusion

A method of illustrating the effects of artificial dissipation in a solution method for the Navier-Stokes equations has been proposed. In this method a flow solution is developed in which the dissipation is that inherent in the method itself, except at the surface, where the transfer of momentum and heat across the wall is determined from the true viscosity and heat conductivity of the fluid being simulated. A boundary layer develops, and the thickness of this boundary layer compared to the thickness of

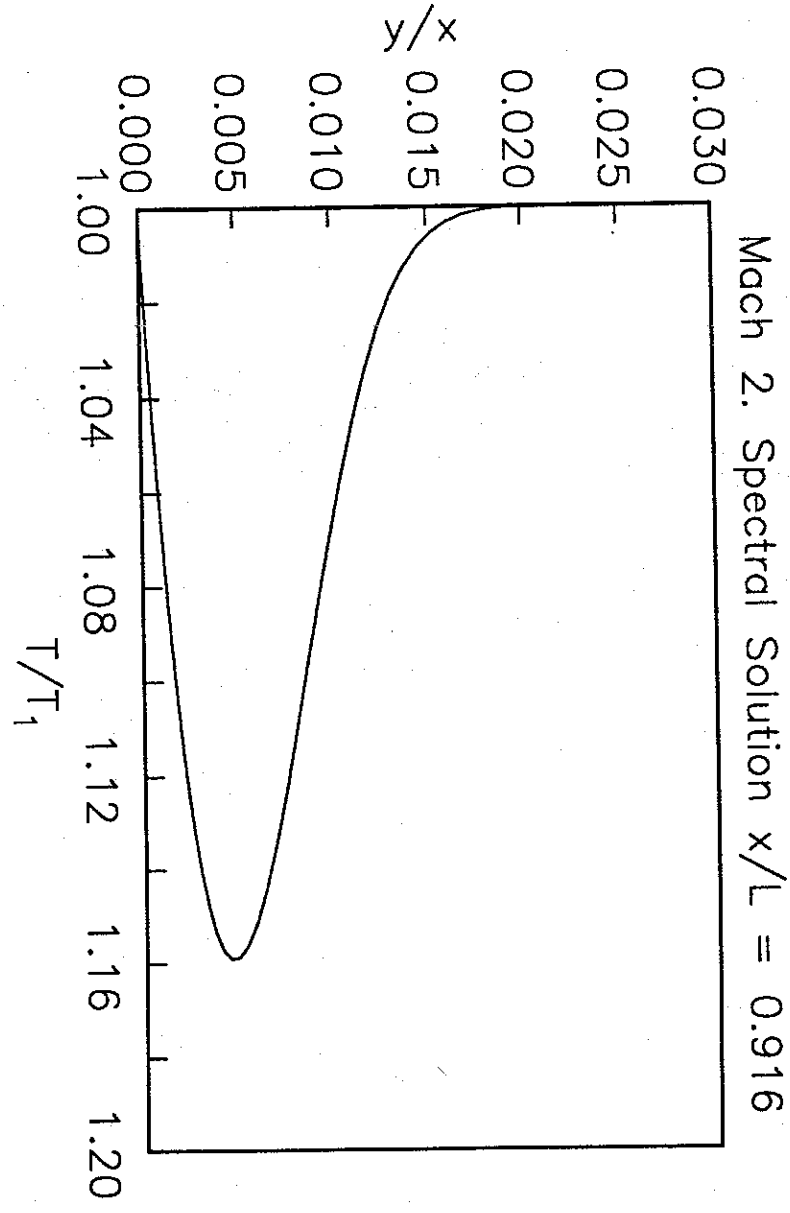

tmp_spec.ps Fri Mar 4 12:13:53 1994

F-5-1

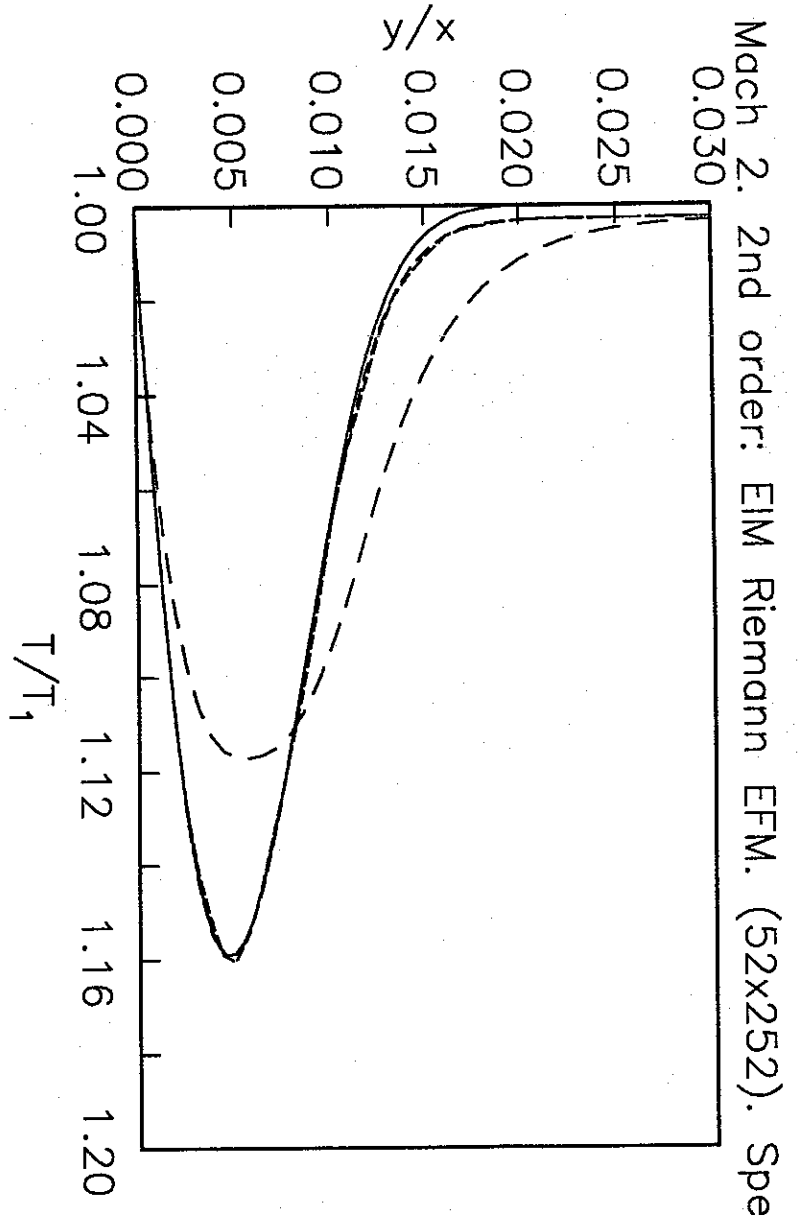

hQMs.ps Sat Mar 5 15:48:28 1994

Fig 4

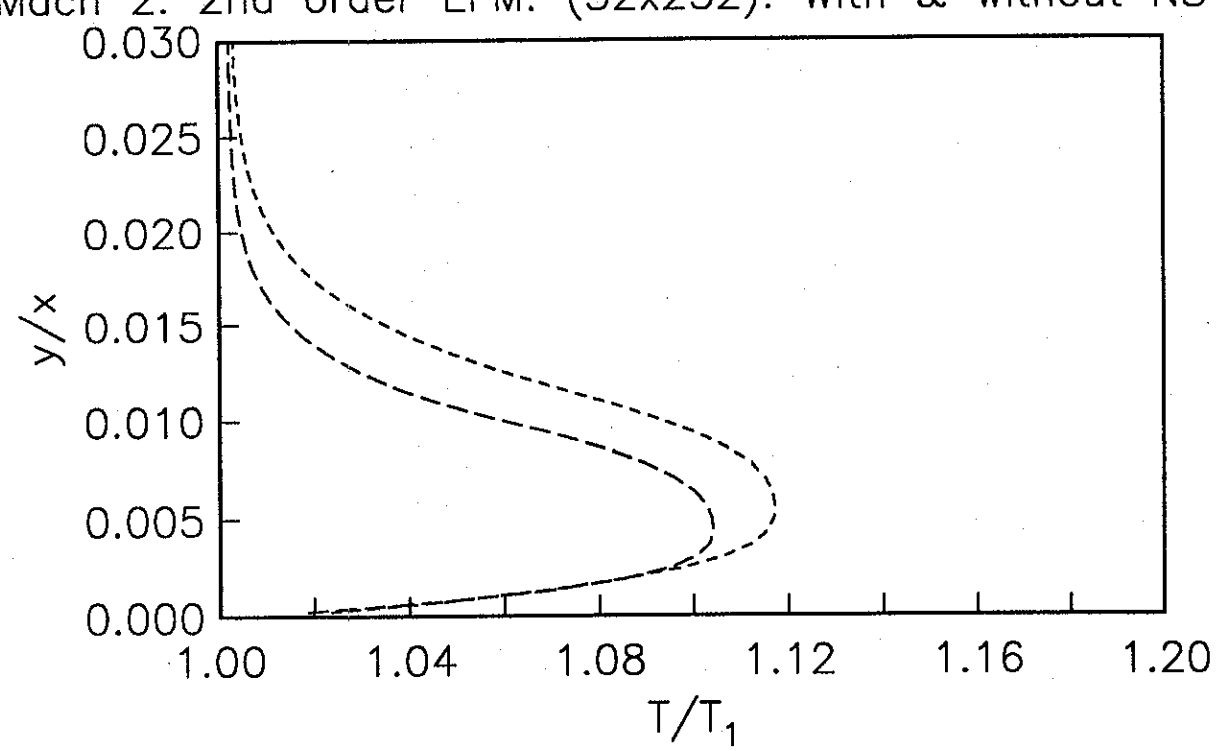

MM0.ps Mon Mar 7 08:35:47 1994

Fig 5

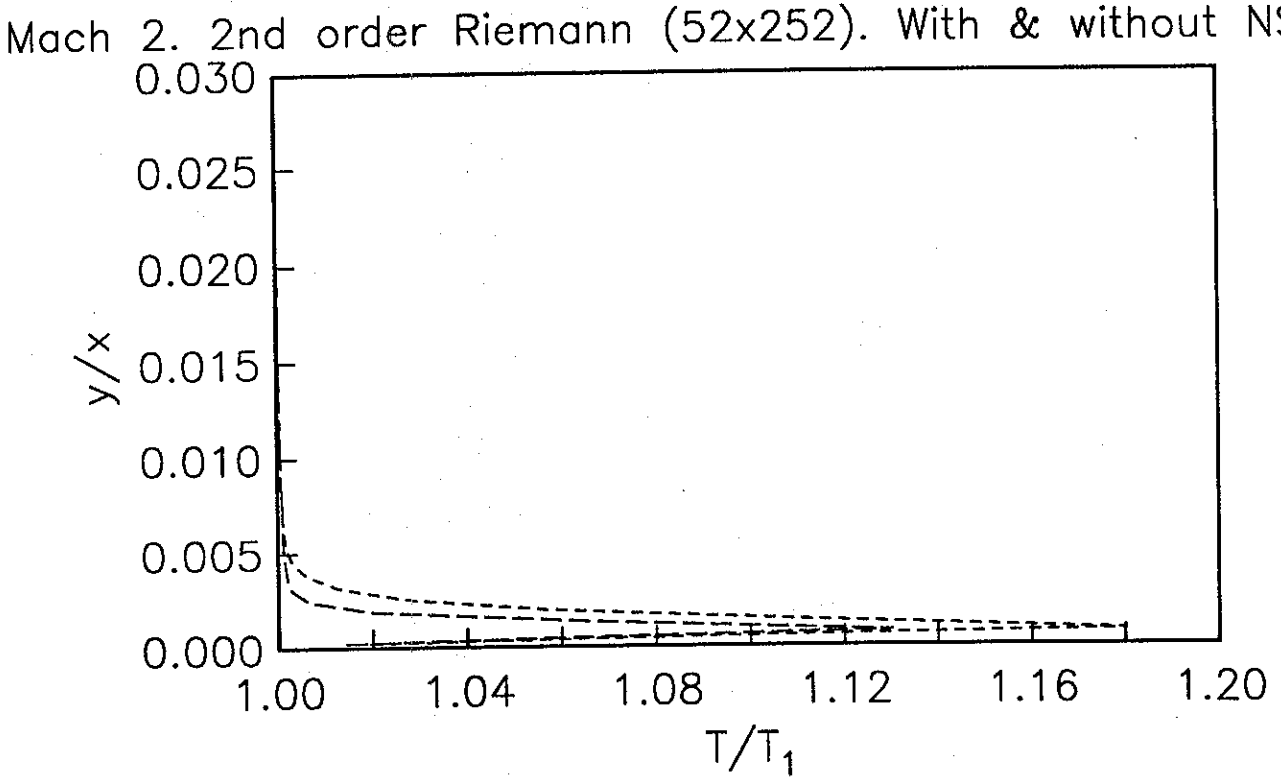

EOQ0.ps Tue Mar 8 15:26:11 1994

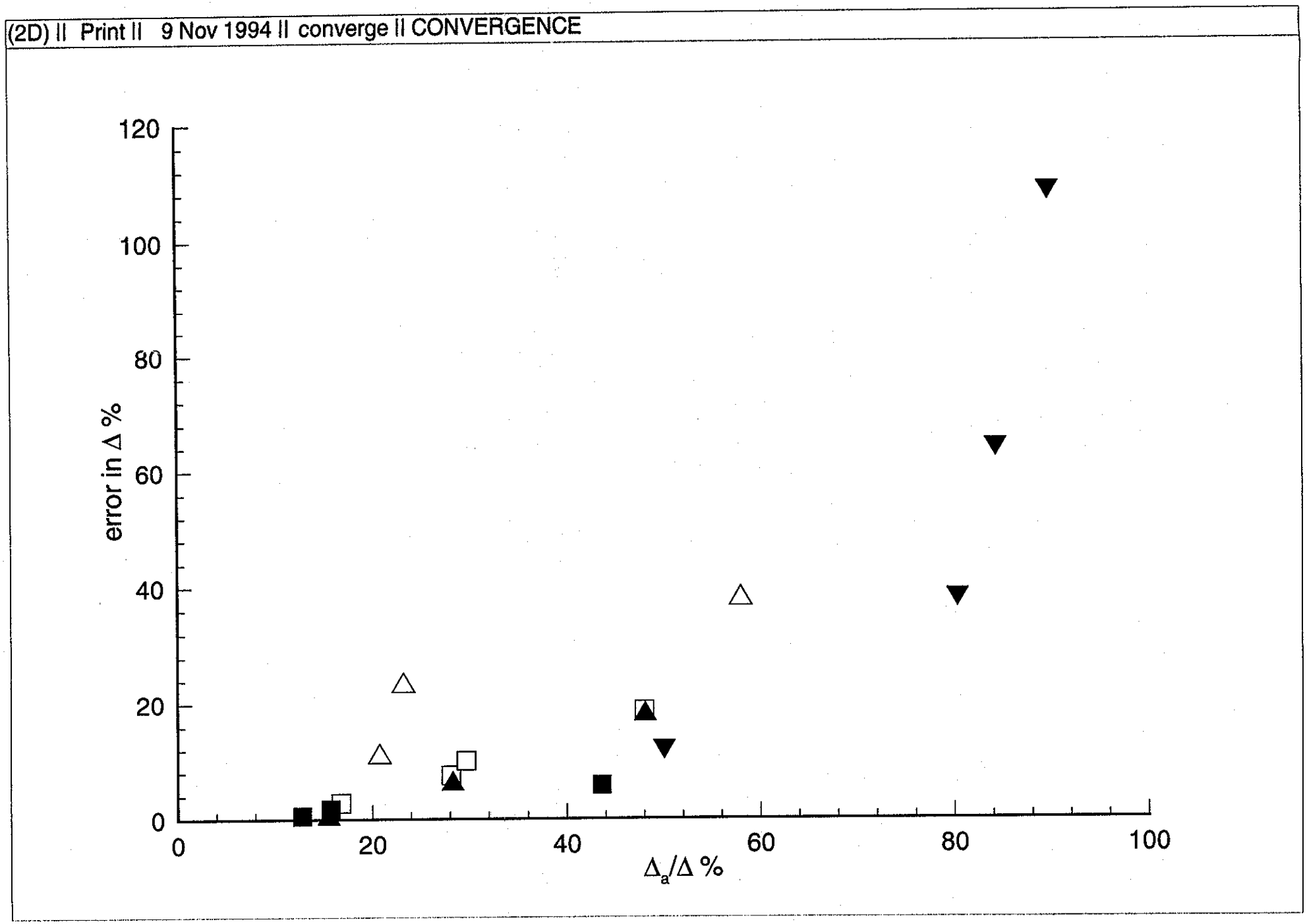
(2D) II Print II 9 Nov 1994 II converge II CONVERGENCE
120
100
80
60
40
20
0
error in Δ %
0
20
40
60
80
100
Δa/Δ %

Fig 6

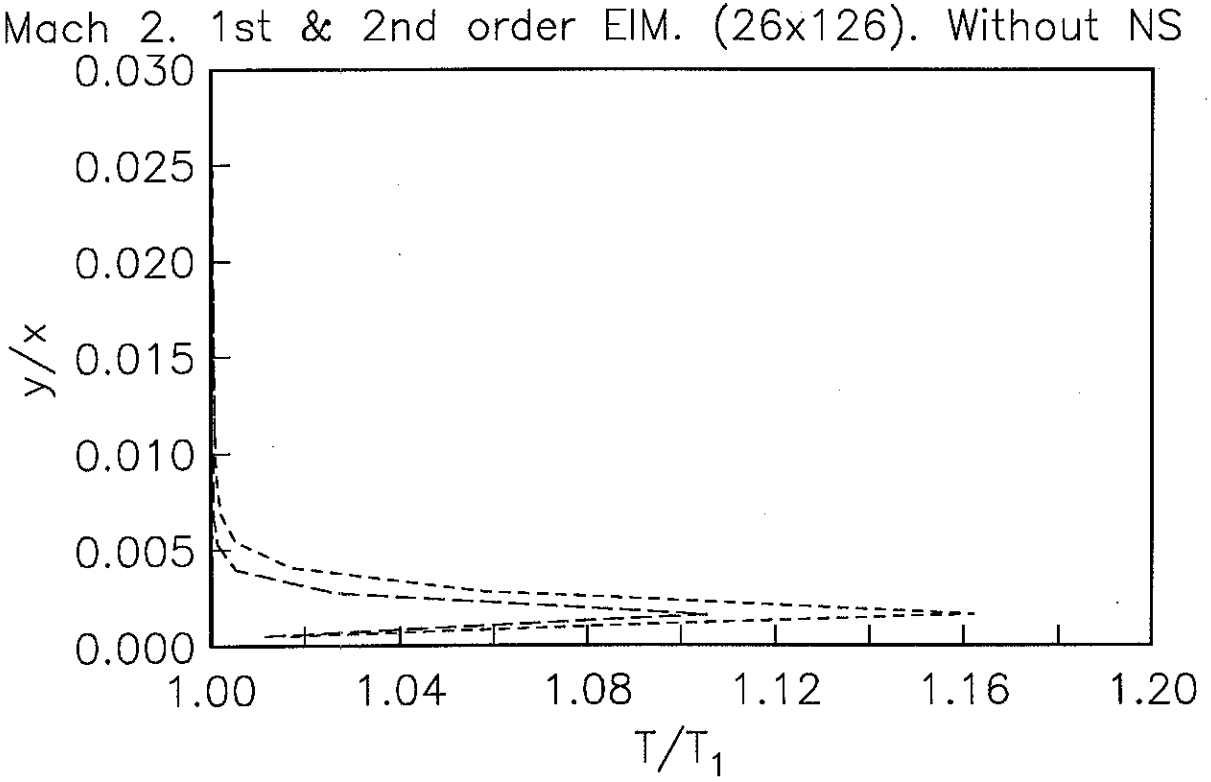

A0H0.ps Mon Mar 7 08:45:43 1994

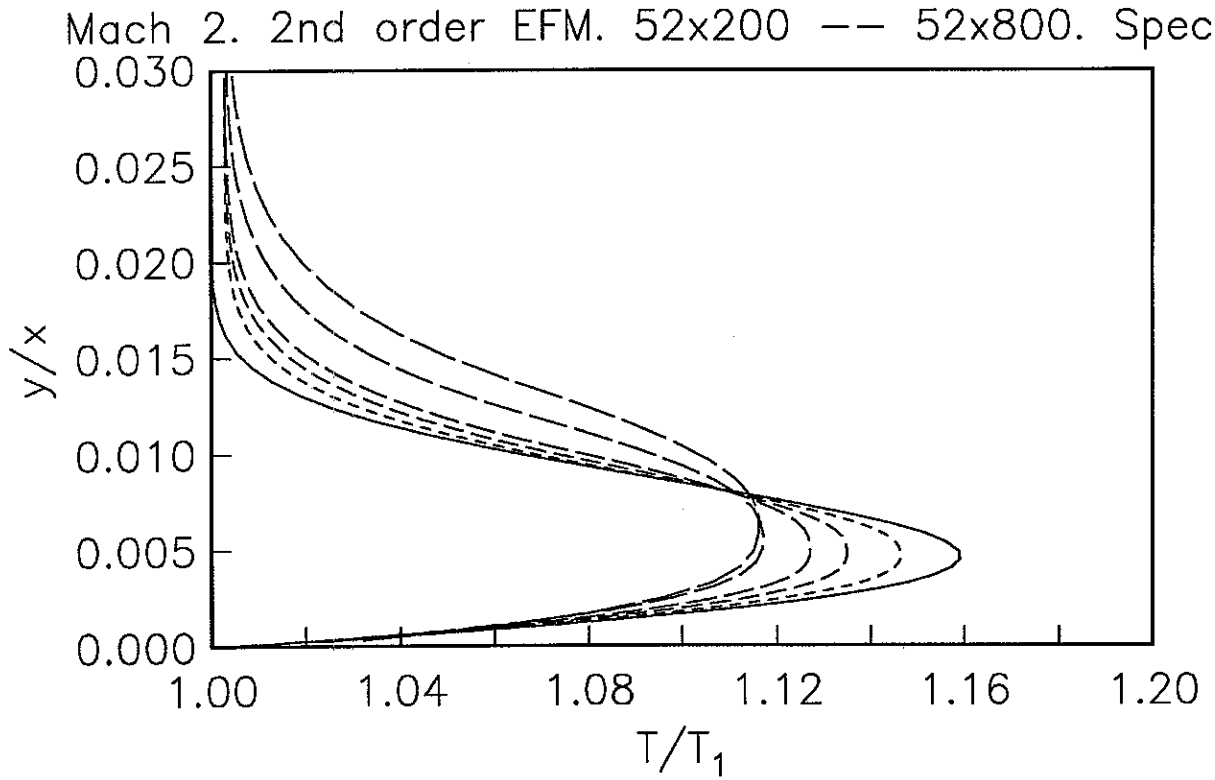

fig7.ps Tue Mar 8 15:35:25 1994

Mach 2. 2nd order EFM. Richardson limit (52x400 – 52x800. Spectral.

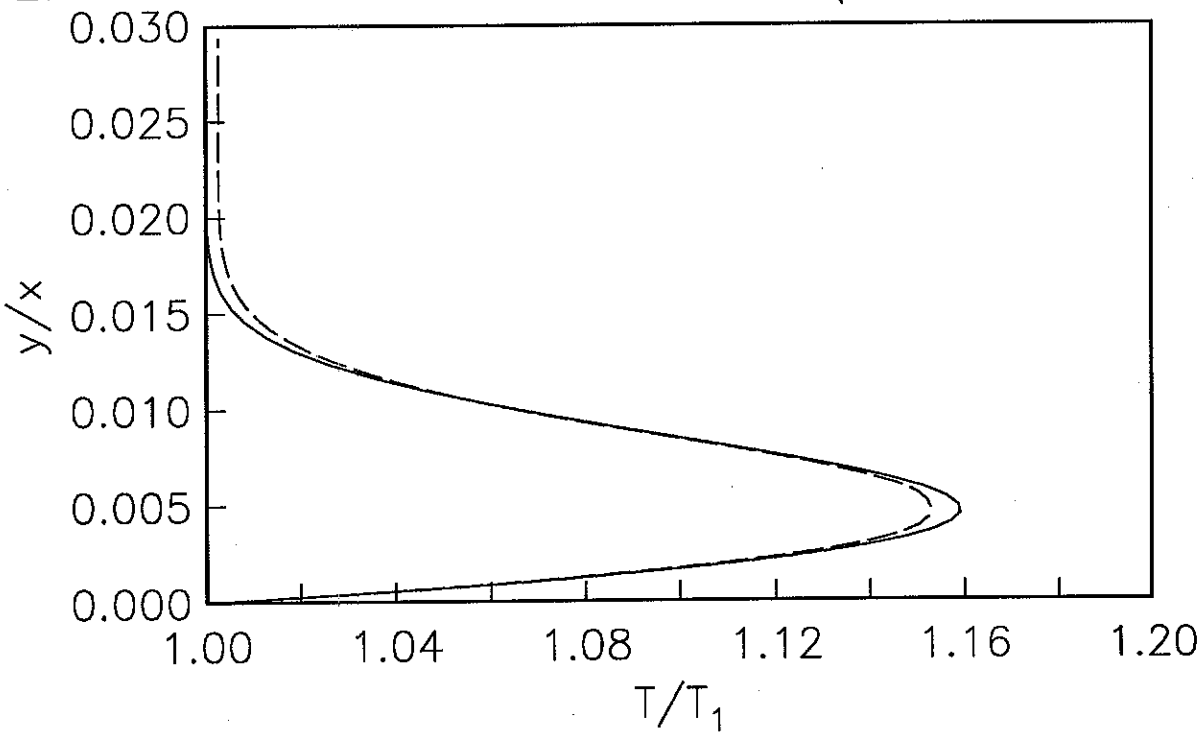

KJ_rs.ps Wed Mar 9 08:27:29 1994

fig9.ps Wed Mar 9 08:43:52 1994